PRAMANA
— journal of
physics

Vol. 41, No. 6,
December 1993
pp. 535–550

Collective bounce-off phenomenon in ^{139}La + Ag(Br) reaction at 1·1 A GeV energy

B SINGH, H S PALSANIA, V KUMAR, K B BHALLA and S LOKANATHAN
Department of Physics, University of Rajasthan, Jaipur 302 004, India

MS received 10 August 1992; revised 12 July 1993

Abstract. Out of a total statistics of 896 ^{139}La + Ag(Br) interactions, 128 interactions having multiplicity of target fragments ($Z \geqslant 1$) $\geqslant 8$ and projectile fragments ($Z \geqslant 2$) $\geqslant 4$ have been selected. They correspond to quasi-peripheral interactions. Azimuthal angle correlation between sources of target fragments (TFs) and projectile fragments (PFs) shows the existence of bounce-off effect. Using data of La + Ag(Br) and ^{84}Kr + Ag(Br) reactions it is shown that individual helium [$Z = 2$, PFs] and heavier fragment [$Z \geqslant 3$, PFs] show different emission characteristics. Further, a two prong correlation function $T(\Phi_{ij})$ plotted for heavier fragments and helium fragments separately, indicates the possibility of existence of different physical conditions. This observation is supported by the different momentum widths of helium fragments and heavier fragments. From the momentum width data of Kr + Ag(Br) reactions normalized density comes out to be $\approx 4{\cdot}7$. Using quasi-elastic kinematics for the bounce-off nuclei, the excitation energy has been computed from the experimental data of flow angles. The strength of bounce-off seems to decrease with the increase of excitation energy or temperature.

Keywords. Collective effects; Bounce-off; momentum-width; quasi elastic scattering kinematics; sqeeze-out; impact parameter; fragmentation; participant region; thermalised source.

PACS No. 25·70

1. Introduction

One of the main objectives of relativistic heavy ion physics is to investigate the equation of state of nuclear matter at abnormally high densities. No model independent method exists to know such densities. Manifestation of high density state in the form of collective flow may provide a way out because it can be detected experimentally.

In the process of compression, impact parameter and the energy of colliding nuclei play a crucial role in changing the density of the overlap region. This in turn affects the strength of the collective effects. About a decade ago the collective effects such as bounce-off at middle range impact parameters were taken up for detailed study. From a large number of preliminary experiments using both symmetric and non-symmetric systems of colliding nuclei such as (i) Ca + Ca at 400 A MeV (ii) Nb + Nb at 400 and 650 A MeV (iii) Au + Au at 150 to 800 A MeV due to Gustaffsson *et al* [1] and Ritter *et al* [2] (iv) U + U at 900 A MeV due to Beavis *et al* [3] (v) Ar + Pb at 400 and 800 A MeV due to Beavis *et al* [3] and Renfordt *et al* [4] (vi) Ar + KCl at 1800 A MeV due to Sandoval *et al* [5] (vii) C + Ag and Ne + U at 393 A MeV energy due to Baumgardt *et al* [6] (viii) U + Ag(Br) at 850 A MeV due to Heckmann *et al* [7] (ix) Kr + Ag(Br) at 1400 A MeV due to Arora *et al* [8] it was concluded that the flow angle depends on both energy and mass of the colliding systems but nothing in specific could be inferred about density of the compressed matter.

On the theoretical side, models such as hydro-dynamical due to Scheid *et al* [9], Baumgardt *et al* [6] and Amsden *et al* [10] and modified cascade model due to Cugnon *et al* [11], Braun and Fraenkel [11] and participant-spectator spallation model due to Gosset *et al* [12] have greatly helped in understanding the general behaviour of the relativistic collisions and the mechanism of the flow effects. Predictions of quantum statistical model due to Stocker *et al* [13] reach closer to the main objective of knowing the equation of state. One of such predictions is that the low temperature and high density conditions are the most favourable conditions for a fragment to grow massive. Although it remains to be tested in a large statistics experiment it seems to be useful for knowing the conditions of the source of fragments.

The phenomenon of bounce-off of nuclei contradicts with the 'on the spot spallation' of colliding nuclei into spectators and participants therefore the spectator-participant model cannot be invoked at the moment of collision. In a relativistic collision, high amount of direct compression takes place in the overlap region and as a result squeeze out of the nuclear matter starts through the non-overlap region. This builds up pressure in this region. As a result of pressure difference in the overlap and non-overlap regions the two regions are separated after a while. The two chunks of nuclear matter are fragmented with distinction in the physical conditions of the two regions. In our earlier short publication due to Palsania *et al* [14] we have identified two physically distinct regions of the projectile nucleus one predominantly decaying into small fragments like helium and the other into big fragments (clubbed into $Z \geqslant 3$ bin) using the La + Ag(Br) reaction data.

In this paper a detailed comparison of Kr + Ag(Br) and La + Ag(Br) reactions has been presented which helps in drawing inferences on emission characteristics. Also, an attempt has been made for the experimental estimation of the density of the most compressed zone using the data of nearly symmetric colliding system i.e. Kr + Ag(Br) reactions.

2. Details of exposure and method of measurements

A stack of G-5 emulsions was exposed to ^{139}La-beam of energy $\approx 1{\cdot}1$ GeV/nucleon at Berkeley Bevatron in April 1983 and in all 896 interactions of La with emulsion nuclei were collected by line scan method. For the present study we have selected 128 interactions having $N_{TF} \geqslant 8$ and $N_{PF} \geqslant 4$, where N_{TF} and N_{PF} are the number of target fragments ($Z \geqslant 1$) and projectile fragments ($Z \geqslant 2$) respectively. These interactions lie within 3 cm but at different lengths from the entry-edge. Therefore, the projectile energy at the point of interaction will be different for all the interactions. The average energy of interacting beam particles for the selected interactions is $\approx 0{\cdot}8$ A GeV. The selected interactions lie within middle layers of emulsion. To avoid effect of emulsion distortions on measurements interactions within 20 μm layer of emulsion from air and glass surface are avoided. It may also be mentioned here that this category of interactions corresponds to neither central nor peripheral interactions as the surviving average number of projectile fragments (PFs) is $6{\cdot}80 \pm 0{\cdot}18$ and target fragments (TFs) is $21{\cdot}10 \pm 0{\cdot}70$. Angle measurements of all PFs and TFs associated with an interaction are done by following the particle track up to a sufficiently long distance and measuring coordinates (X, Y, Z) at more than two positions. Using dip and projected angles of each track, components of unit vector of each track ($\hat{r}_X, \hat{r}_Y, \hat{r}_Z$) are evaluated to give the principal unit vector of emission for PFs ($\hat{r}_{PF}$) and TFs ($\hat{r}_{TF}$) separately. Either

from the number of PFs or TFs the unit principal vector can be written as

$$\hat{r} = \frac{\left\{\sum_{}^{n} r_X\right\}\hat{i} + \left\{\sum_{}^{n} r_Y\right\}\hat{j} + \left\{\sum_{}^{n} r_Z\right\}\hat{k}}{\left[\left\{\sum_{}^{n} r_X\right\}^2 + \left\{\sum_{}^{n} r_Y\right\}^2 + \left\{\sum_{}^{n} r_Z\right\}^2\right]^{1/2}} \tag{1}$$

$$= R_X\hat{i} + R_Y\hat{j} + R_Z\hat{k} \tag{2}$$

where $n = N_{PF}$ when unit principal vector $\hat{r}_{PF}$ is computed and $n = N_{TF}$ when $\hat{r}_{TF}$ is computed. Thus, for an event two principal vectors are determined. These principal vectors provide direction of flow of nuclear matter related to projectile and target respectively to a reasonable accuracy because of the following reasons i) all fragments are likely to have identical to beam momentum as on fragmentation they acquire a small $P_T \approx 70$–80 MeV c/n only. Similarly amongst the TFs most of them are evaporated fragments and ii) a large number of fragments are used to determine the principal vectors. The average number of them is indicated earlier.

3. Experimental results and discussion

3.1 *Bounce-off effect*

Distributions of the flow angle of the PFs and TFs deduced from their respective principal vectors on event-by-event basis for La + Ag(Br) reaction have been presented in our earlier paper [14] the average values of the flow angles of PFs ($=\bar{\theta}_{PF}$) and TFs($=\bar{\theta}_{TF}$) in La + Ag(Br) reaction at 0·8 A GeV, Kr + Ag(Br) at 1·27 A GeV, ^{238}U + Ag(Br) at 0·85 A GeV and ^{56}Fe + Ag(Br) at 1·88 A GeV [15] have been given in table 1 for comparison. Collective flow of nuclear matter of relativistic projectile at such a large angle ($\approx 3°$) shows the existence of a strong nuclear collective effect. Contribution of coulomb scattering to the flow angle has been shown [7,8] to be negligibly small. From the data of $\bar{\theta}_{PF}$ given in table 1 it is clear that the flow angle decreases with increasing projectile energy. It can be pointed out that $\bar{\theta}_{TF}$ has been evaluated from an average of 21 charged target fragments and existence of flow angle as large as $\approx 31°$ cannot have large spurious error due to limited number of particles. Thus, both $\bar{\theta}_{PF}$ and $\bar{\theta}_{TF}$ can be treated as the clear indications of collective flow.

To investigate the correlated scattering of colliding nuclei, the difference of azimuthal angles $\Delta\Phi = |\Phi_{TF} - \Phi_{PF}|$ of the principal vectors of TFs and PFs for La + Ag(Br) interactions has been analysed. In figure 1 results of the Monte-Carlo, corresponding to no correlation situation obtained by random generation of the azimuthal angle of each fragment, have also been displayed along with experimental results of $\Delta\Phi$. The numerical values of $\overline{\Delta\Phi}$ obtained from the present data have been compared with those of Kr + Ag(Br), U + Ag(Br) and Fe + Ag(Br) in table 1. It may be mentioned that due to the increase of number of events of Kr + Ag(Br) reactions some of the results presented here have changed slightly as compared to that given in [8]. The strength of back-to-back correlation may be defined by the ratio, R i.e. the ratio of number of events with $\Delta\Phi \geqslant 90°$ to $\Delta\Phi < 90°$. In table 1 R has been given for different colliding systems and it may be noted that R is very high (≈ 24) in U + Ag(Br) reaction as compared to $\approx 2{\cdot}2$ for La + Ag(Br) reaction. It may be inferred from the

Table 1. Comparison of the averages of the flow angle of PFs ($\bar{\theta}_{PF}$) and TFs ($\bar{\theta}_{TF}$); $\overline{\Delta\Phi}$; R; F/B-ratio of TFs; excitation energy E^*.

Property	La + Ag(Br)[14] at 0·8 A GeV	Kr + Ag(Br)[8] at 1·27 A GeV	U + Ag(Br)[7] at 0·85 A GeV	Fe + Ag(Br)[15] at 1·88 A GeV
$\bar{\theta}_{PF}(Z \geqslant 2)$	$2{\cdot}87 \pm 0{\cdot}24°$	$2{\cdot}03 \pm 0{\cdot}14°$	$2{\cdot}35 \pm 0{\cdot}20°$	—
$\bar{\theta}_{TF}(Z \geqslant 1)$	$30{\cdot}39 \pm 1{\cdot}66°$ ($N_{TF} \geqslant 8, N_{PF} \geqslant 4$)	$32{\cdot}86 \pm 1{\cdot}29°$ ($N_{TF} \geqslant 8, N_{PF} \geqslant 4$)	$47{\cdot}10 \pm 2{\cdot}10°$ ($N_{TF} \geqslant 10, N_{PF} \geqslant 8$)	$43{\cdot}20 \pm 1{\cdot}80°$ ($N_{TF} \geqslant 9$)
$\overline{\Delta\Phi} = \langle\lvert\Phi_{TF} - \Phi_{PF}\rvert\rangle$	$114{\cdot}84 \pm 4{\cdot}51°$	$107{\cdot}24 \pm 4{\cdot}32°$	$146{\cdot}00 \pm 4{\cdot}00°$	$101{\cdot}00 \pm 1{\cdot}80°$
R	$2{\cdot}20 \pm 0{\cdot}34$	$1{\cdot}74 \pm 0{\cdot}24$	$23{\cdot}5 \pm 3{\cdot}63$	—
F/B-ratio Obs.	$5{\cdot}42 \pm 0{\cdot}22$	$4{\cdot}74 \pm 0{\cdot}18$	$5{\cdot}94 \pm 0{\cdot}51$	—
Corr.	$4{\cdot}88 \pm 0{\cdot}20$	$4{\cdot}84 \pm 0{\cdot}04$	$5{\cdot}28 \pm 0{\cdot}46$	—
E^*	7·13 GeV	4·90 GeV	5·80 GeV	—

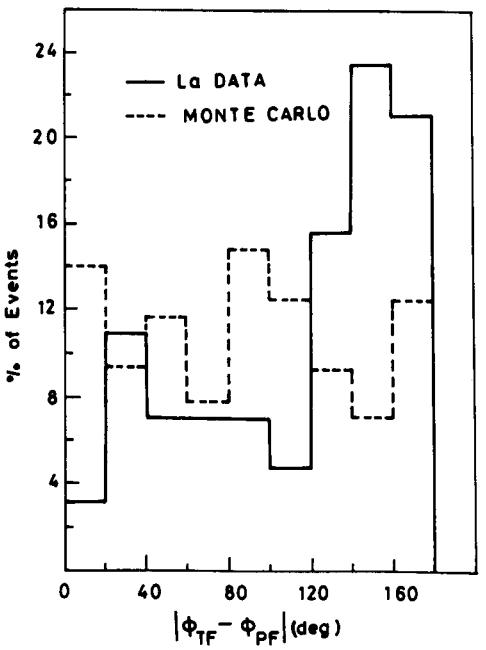

Figure 1. A plot of the difference of azimuthal angles of principal vector of TFs and PFs on event-by-event basis. The dashed line shows no correlation Monte-Carlo (MC) of La + Ag(Br) collision. The MC corresponds to $\overline{\Delta\Phi}(MC) = 87{\cdot}81 \pm 4{\cdot}67°$ and dispersion $D = 52{\cdot}28 \pm 3{\cdot}27°$.

data that the strength of back-to-back correlation in the azimuthal plane shows dependence on the mass of the colliding system.

3.2 *Emission characteristics*

To study the emission characteristics of bounce-off nuclei, projections of angle θ' (taken separately for helium and heavier fragments) onto the plane containing the principal vector of the PFs have been considered. Here θ' is the angle of a fragment vector with respect to its principal vector. The width of the $dN/d\theta'$ (proj.) distribution corresponds to the momentum width of nucleons in the fragmenting source. Frequency plots of θ'_{He}(proj.) for helium fragments ($Z = 2$) and θ'_{F}(proj.) for $Z \geqslant 3$ projectile – fragments for La + Ag(Br) reactions have been presented in [14]. Similar plots have been made for Kr + Ag(Br) data. Characteristics of these distributions such as dispersion and peakness have been given in table 2 for both the reactions for comparison. It may be noted that there exists difference in the values of dispersion and peakness for helium fragments and heavier fragments in both the reactions. Both helium and heavier fragments show peakness much higher than 3, that is the peakness of a standard gaussian distribution, in both cases of reactions. It may therefore, be inferred that majority of helium as well as heavier fragments are emitted from two different zones or sources of different physical conditions. The values of momentum-width given in table 2 have been computed using the initial beam momentum and the dispersion of θ'(proj.) distribution as given in the first row of table 2. Data of peripheral interactions of Kr + Ag(Br) reactions ($N_h = 0, 1$ events) are given in the last column of table for comparison with the bounce-off events. In general, it can be inferred that

Table 2. Dispersion and peakness of θ'_{He}(proj.) and θ'_{F}(proj.) distributions for La + Ag(Br) and Kr + Ag(Br) reactions. The momentum width has been calculated using the beam momentum and dispersion data.

	La + Ag(Br) at 0·8 A GeV (All b.o. events)		Kr + Ag(Br) at 1·27 A GeV (All b.o. events)		Kr + Ag(Br) at 1·27 A GeV (Peripheral events)	
Property	Helium fragments	Heavier fragments	Helium fragments	Heavier fragments	Helium fragments	Heavier fragments
Dispersion	2·99 ± 0·09°	2·52 ± 0·11°	2·31 ± 0·07°	2·27 ± 0·1°	1·39 ± 0·1°	1·66 ± 0·2°
Peakness	4·32	7·76	5·36	6·01	3·26	8·53
Momentum width (MeV/c/n)	76·13 ± 2·29	64·18 ± 2·44	79·24 ± 2·44	77·87 ± 3·48	46·67 ± 3·48	56·93 ± 7·31

heavier fragments ($Z \geqslant 3$) have much higher values of peakness compared to that of helium fragments showing the lack of degree of randomness. It may also be said that after collision a big chunk of the nuclear matter even on fragmentation has high coherence. In bounce-off events, widths of helium fragments are in general higher than that of heavy fragments. This is probably because of high modification of original Fermi momentum of a highly compressed part of the projectile nucleus during the collision. Thus, we can make use of the ratio of momentum-widths (σ's) of He-fragments in bounce-off events to that in peripheral events to find out the ratio of densities (ρ) (see Appendix)

$$\frac{\rho_{\text{b.o.}}}{\rho_{\text{Peri}}} = \frac{(\sigma_{\text{b.o.}})^3}{(\sigma_{\text{Peri}})^3}. \tag{3}$$

Here, we assume that in peripheral collision ($N_h = 0, 1$ events) compression of the projectile is insignificant compared to the bounce-off mode. For nearly symmetric collision i.e. Kr + Ag(Br) reactions $\rho_{\text{b.o.}}/\rho_{\text{Peri}} = (79/47)^3 = 4{\cdot}7$. This agrees well with the ratio $\approx 4{\cdot}5$ for the krypton reaction obtained from the relation by Stocker *et al* [16, 17].

Assuming that the target after the bounce-off, gets only a small negligible momentum it is easy to study the forward to backward ratio of the target fragments from the $\cos\theta'_{\text{TF}}$ plots. Here θ'_{TF} is the space-angle of a target fragment with respect to the principal vector of TFs. In figure 2 plots between the logarithm of frequence and $\cos\theta'_{\text{TF}}$ have been given for La + Ag(Br) and Kr + Ag(Br) reactions. The slope of the straight line ($= b$) fitted to the data gives the F/B-ratio [$F/B = \exp(b)$] following the non-relativistic Maxwell–Boltzmann distribution of momentum of nucleons in the target nucleus [7]. In table 1 values of F/B-ratio have been given for La + Ag(Br), Kr + Ag(Br) and U + Ag(Br) reactions. In all the cases F/B-ratio comes out to be much greater than unity confirming the existence of flow of target matter. The corrected value of the F/B-ratio for the two reactions is also given in table. As pointed out by Heckmann *et al* [7] the correction factor $f = [(F/B)_{\text{obs.}}/(F/B)_{\text{MC}}]$ has been estimated by finding out $(F/B)_{\text{Corr.}}$ by Monte-carlo (MC) simulation of 128 events assuming

$$\frac{\mathrm{d}N}{\mathrm{d}(\cos\theta')} \propto \exp(b\cos\theta')$$

distribution with $\theta' = (R_X \times r_x) + (R_Y \times r_y) + (R_Z \times r_z)$. Here R_X, R_Y and R_Z are the three components of empirically determined unit principal vector $\hat{r}_{\text{TF}}$. The fragment vectors r_x, r_y and r_z have been generated randomly and to encompass the range of $(F/B)_{\text{obs}}$ the value of b has also been chosen randomly so that F/B falls in between 4·25 and 7·0. The combined result of 20 times Monte-carlo of each event gives $(F/B)_{\text{MC}} = 4{\cdot}88 \pm 0{\cdot}06$. Thus the corrected value of F/B-ratio can be given by

$$(F/B)_{\text{Corr}} = \left(\frac{1}{f}\right)(F/B)_{\text{Obs}} = 4{\cdot}88 \pm 0{\cdot}20.$$

In figure 2 the lines corresponding to $(F/B)_{\text{Corr}}$ have also been shown for both the reactions. In particular for La + Ag(Br) reaction the slope of the line (MC), $b = 1{\cdot}585$.

In has been shown [7, 8, 14] that the bounce-off nuclei follow the quasi-elastic scattering (QES) kinematics wherein it is assumed that both projectile and target

nuclei share equal amount of excitation energy (E^*). In figure 3a $\bar{\theta}_{PF}$ versus $\bar{\theta}_{TF}$ plots for La + Ag(Br) and Kr + Ag(Br) reactions have been given. The curves correspond to the QES at a particular value of E^* fitted to the experimental data of $\bar{\theta}_{PF}$ and $\bar{\theta}_{TF}$ of the reaction. Values of E^* so obtained for La + Ag(Br), Kr + Ag(Br) and U + Ag(Br) reactions are given in table 1. It may be inferred that excitation energies, although different in different reactions, are very high in all the three cases. The difference in E^* values may arise because of different ranges of impact parameters in the three reactions as selection of events at required impact parameter is difficult in emulsion experiments.

In the event of bounce-off of colliding nuclei, at different impact parameters the size of overlap region (so called participant region) will increase with the decrease of impact parameter. In the relatively more compressed overlap region the emission characteristics are likely to change with the conditions of compression. We know that mostly the grey particles ($\bar{N}_g$) are the recoiled target protons with velocity $\beta = 0{\cdot}3$

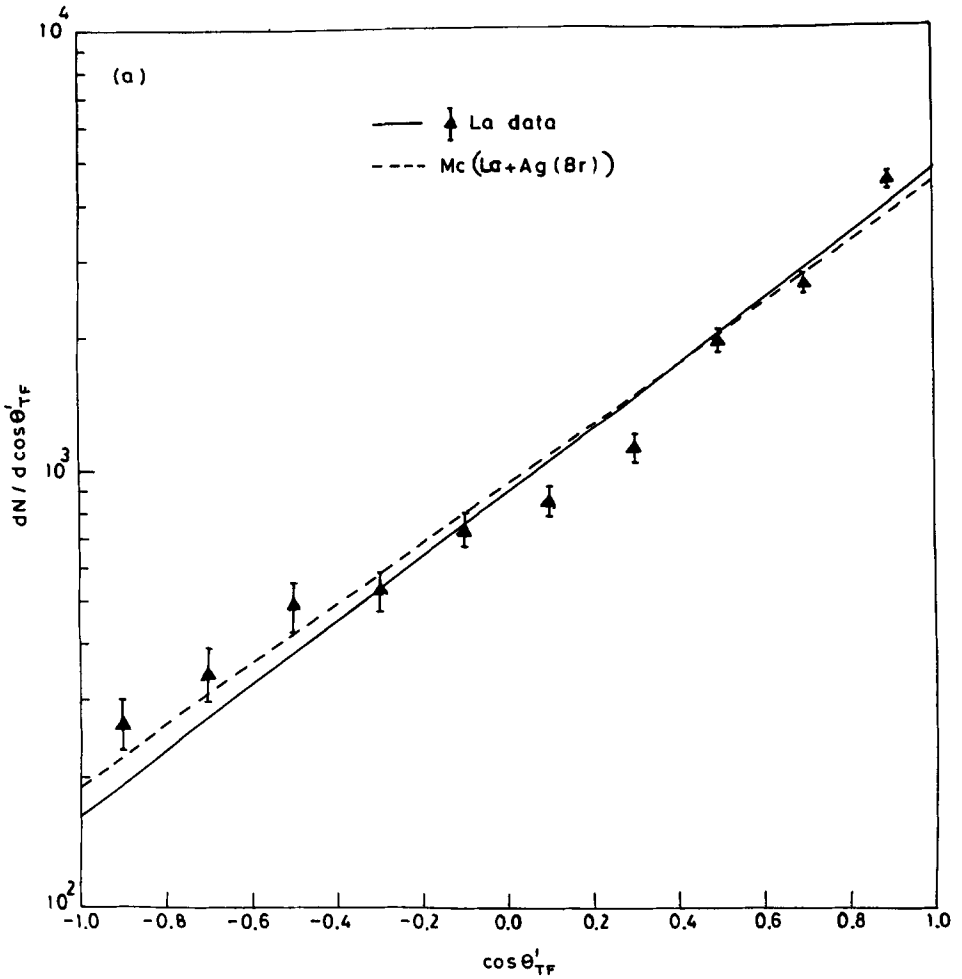

Figure 2a. $\ln(dN/d\cos\theta'_{TF})$ versus $\cos\theta'_{TF}$ plot of the target fragments for La + Ag(Br) (▲) reaction. The slope of line through data is to $b = \ln(F/B)_{Obs} = 1{\cdot}69 \pm 0{\cdot}04$. Dashed line corresponds to Monte-Carlo calculations with $b = 1{\cdot}585$ which reproduces the experimental data.

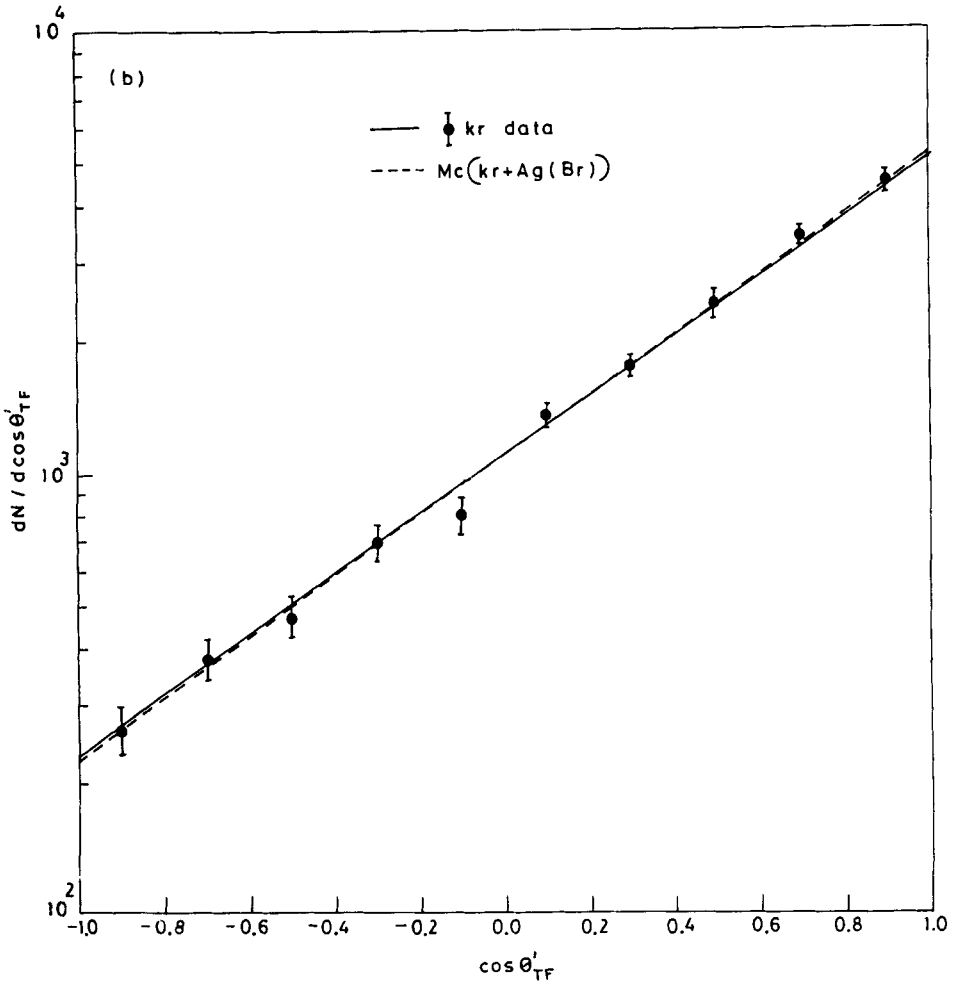

Figure 2b. $\ln(dN/d\cos\theta'_{TF})$ versus $\cos\theta'_{TF}$ plot of the target fragments for Kr + Ag(Br) (●) reaction. The slope of the line through data is to $b = 1{\cdot}55 \pm 0{\cdot}04$ and the dashed line (MC) corresponds to $b = 1{\cdot}578$.

to 0·7 and their number increases with the decrease of impact parameter. In a way, qualitatively speaking, their number represents the size of the participant region. In an attempt to study the effect of density and temperature on collective bounce-off effect, we divide the data of 68 La + Ag(Br) interactions (measurements of these interactions are doubly checked) into the following three categories in order of decreasing size of participant or increasing size of spectator chunk,

(i) $1 \leqslant N_{He} \leqslant 3[\bar{N}_g = 13{\cdot}55 \pm 1{\cdot}80$ or smaller projectile spectator]

(ii) $4 \leqslant N_{He} \leqslant 6[\bar{N}_g = 10{\cdot}94 \pm 0{\cdot}80$ or bigger projectile spectator]

(iii) $N_{He} \geqslant 7[\bar{N}_g = 8{\cdot}86 \pm 1{\cdot}10$ or biggest projectile spectator]

Various characteristics of events such as their number N, average multiplicities of helium and heavier fragments, greys, total target fragments, average space angle of helium fragments, PFs and TFs, azimuthal difference $\overline{\Delta\Phi}$, strength of back-to-back correlation, F/B-ratio of TFs and the excitation energy related to the above three

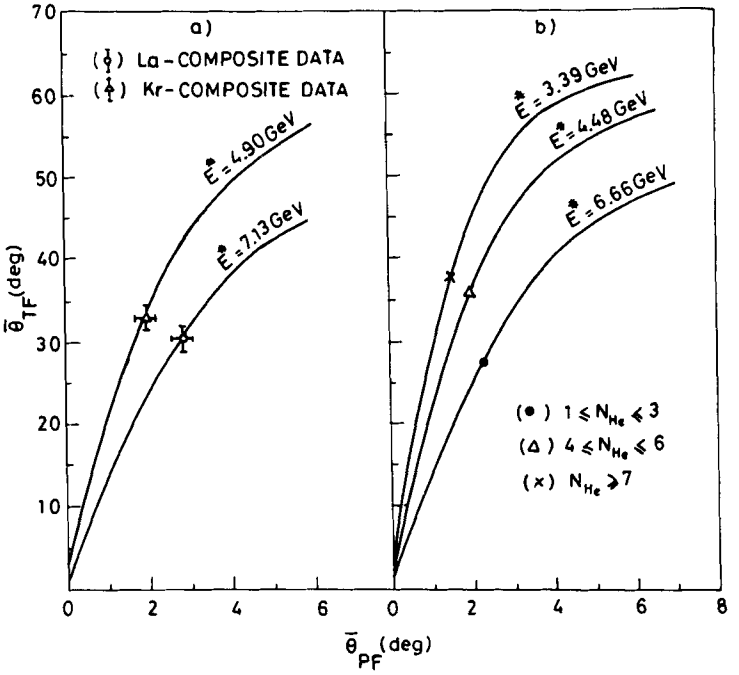

Figure 3. Plots between angles $\bar{\theta}_{PF}$ and $\bar{\theta}_{TF}$ for the (**a**) composite data of La + Ag(Br) and Kr + Ag(Br) reactions separately and for (**b**) three categories $1 \leqslant N_{He} \leqslant 3$, $4 \leqslant N_{He} \leqslant 6$ and $N_{He} \geqslant 7$ of the La + Ag(Br) data. The curves in the figure a) and b) correspond to the quasi elastic scattering (QES) kinematics.

Table 3. Data of various characteristics of events belonging to three categories in the case of La + Ag(Br) collision. The $\bar{\theta}_{He}$ is the space angle of helium fragments with respect to beam direction. *F/B*-ratio means Forward to Backward ratio of TFs ($Z \geqslant 1$) with respect to direction of their principal vector.

Property	$1 \leqslant N_{He} \leqslant 3$	$4 \leqslant N_{He} \leqslant 6$	$N_{He} \geqslant 7$
N^* (Events)	17	36	14
$\bar{N}_{He}$	$2{\cdot}71 \pm 0{\cdot}66$	$4{\cdot}92 \pm 0{\cdot}82$	$8{\cdot}00 \pm 2{\cdot}14$
$\bar{N}_F$	$2{\cdot}06 \pm 0{\cdot}50$	$1{\cdot}97 \pm 0{\cdot}33$	$1{\cdot}36 \pm 0{\cdot}36$
$\bar{N}_F/\bar{N}_{He}$	0·76	0·40	0·17
$\bar{N}_g$	$13{\cdot}55 \pm 1{\cdot}80$	$10{\cdot}94 \pm 0{\cdot}80$	$8{\cdot}86 \pm 1{\cdot}10$
$\bar{N}_{TF}$	$23{\cdot}47 \pm 5{\cdot}70$	$22{\cdot}97 \pm 3{\cdot}83$	$20{\cdot}29 \pm 5{\cdot}42$
$\bar{\theta}_{He}$	$4{\cdot}31 \pm 0{\cdot}64°$	$4{\cdot}04 \pm 0{\cdot}30°$	$3{\cdot}41 \pm 0{\cdot}32°$
$\bar{\theta}_{PF}$	$2{\cdot}24 \pm 0{\cdot}54°$	$1{\cdot}97 \pm 0{\cdot}33°$	$1{\cdot}50 \pm 0{\cdot}40°$
$\bar{\theta}_{TF}$	$27{\cdot}35 \pm 6{\cdot}63°$	$36{\cdot}11 \pm 6{\cdot}02°$	$38{\cdot}27 \pm 10{\cdot}23°$
$\overline{\Delta\Phi} = \langle \lvert\Phi_{TF} - \Phi_{PF}\rvert \rangle$	$119{\cdot}80 \pm 11{\cdot}80°$	$125{\cdot}90 \pm 8{\cdot}01°$	$133{\cdot}70 \pm 13{\cdot}06°$
R	$3{\cdot}25 \pm 0{\cdot}85$	$3{\cdot}00 \pm 0{\cdot}65$	$6{\cdot}00 \pm 1{\cdot}58$
F/B-ratio	$5{\cdot}76 \pm 0{\cdot}63$	$5{\cdot}37 \pm 0{\cdot}41$	$4{\cdot}69 \pm 0{\cdot}58$
E^*	6·66 GeV	4·48 GeV	3·39 GeV

*Out of 68 events, one is with $N_{He} = 0$.

categories are given in tables 3 and 4. The following observations can be made from the data,

(a) that the events of category (i) show an enhanced average number of fragments ($Z \geqslant 3$), $\bar{N}_F$ than the events in categories (ii) and (iii). It may be mentioned that in this experiment projectile fragments with $Z = 1$ have not been identified hence not included in the study. The number of such fragments would be much larger in category (i) compared to the other two categories.
(b) The average values of $\bar{\theta}_{PF}$ and $\bar{\theta}_{TF}$ corresponding to principal vector of events show significant difference in the three categories. For example, $\bar{\theta}_{PF}$ being larger in category (i) implies larger transverse momentum of the PFs. In a scattering, transverse momentum of projectile source is balanced by the corresponding recoil of target at $\bar{\theta}_{TF}$ angle. This means that the three momentum of the target should be higher in events of category (i) than in categories (ii) and (iii). Using the experimental value of $\bar{\theta}_{TF}$ given in table 3, P_{recoil} comes out to be 22·11, 17·24 and 16·4 GeV/c in categories (i), (ii) and (iii) respectively. In addition, it also indicates that the size of overlap region is biggest in category (i) and smallest in category (iii) as assumed earlier. Calculating the excitation energy E^* from the data of $\bar{\theta}_{PF}$ and $\bar{\theta}_{TF}$, one sees a remarkable difference i.e. $E^* \approx 6{\cdot}66$ GeV for category (i), 4·48 GeV for category (ii) and 3·39 GeV for category (iii). For comparison, figure 3b gives the plots between $\bar{\theta}_{PF}$ and $\bar{\theta}_{TF}$ for the three categories of events, deduced from QES kinematics alongwith the experimental data. On the other hand back-to-back correlation of colliding nuclei has also been studied for the events of three categories and the values of $\overline{\Delta\Phi}$ and R have been calculated from the experimental data. The values of $\overline{\Delta\Phi}$ and R come out to be 119·8° and 3·25 for category (i), 125·9° and 3·0 for category (ii) and 133·7° and 6·0 for category (iii) respectively. Events corresponding to category (iii) exhibit the strongest bounce-off behavior and on reduction in the impact parameter in categories (ii) and (iii) there is significant reduction in the effect. Difference in the values of E^* for the three categories arises because of varying potential energy due to more compression and rescattering at different impact parameters than at large impact parameters.
(c) From the data of momentum width given in table 4 it is evident that the width in helium PFs is in general higher than that of $Z \geqslant 3$ PFs and there is a gradual enhancement in the width when we go from large impact parameter collision (i.e. category (iii)) to smaller impact parameter collision i.e. category (i). Intuitively, this supports the relationship between σ^2 and $\langle P^2 \rangle$ and hence between density and width deduced in Appendix.

3.3 *Azimuthal correlation between alphas and fragments*

Two particles close in space, time and momentum are expected to be correlated. The correlation between heavier ($Z \geqslant 3$) and helium fragments can be studied to some extent following the method given by Koonin [18]. The following simplified two prong azimuthal angle correlation function given by Jakobsson [19] is generally used for this purpose,

$$C(\Phi_{ij}) = 2T(\Phi_{ij}) - \langle n \rangle^2 / 2\pi \tag{4}$$

where $T(\Phi_{ij}) = (\pi/N)\mathrm{d}N/\mathrm{d}\Phi_{ij}; \Phi_{ij} = |\Phi_i - \Phi_j|$ and $\langle n \rangle$ is the mean multiplicity of prongs used for the purpose of correlation. Φ_i and Φ_j are the azimuthal angles of particle i and j respectively. N is the total number of pairs of two prongs. The relation

Table 4. Data of various characteristics such as dispersion, peakness and momentum width of θ'_{He}(proj) and θ'_{F}(proj) distributions of events belonging to three categories of La + Ag(Br) reaction. The momentum width has been calculated using the beam momentum and dispersion data.

	$1 \leqslant N_{He} \leqslant 3$		$4 \leqslant N_{He} \leqslant 6$		$N_{He} \geqslant 7$	
Property	Helium	Frag.'s	Helium	Frag.'s	Helium	Frag.'s
Dispersion	$2{\cdot}96 \pm 0{\cdot}31°$	$2{\cdot}31 \pm 0{\cdot}27°$	$2{\cdot}77 \pm 0{\cdot}18°$	$2{\cdot}01 \pm 0{\cdot}17°$	$2{\cdot}39 \pm 0{\cdot}16°$	$1{\cdot}09 \pm 0{\cdot}18°$
Peakness	3·37	6·39	3·61	6·44	3·11	3·67
Momentum width (MeV/c/n)	$75{\cdot}37 \pm 7{\cdot}9$	$58{\cdot}83 \pm 6{\cdot}9$	$70{\cdot}53 \pm 4{\cdot}6$	$51{\cdot}19 \pm 4{\cdot}3$	$60{\cdot}87 \pm 4{\cdot}1$	$27{\cdot}76 \pm 4{\cdot}6$

*Out of 68 events one is with $N_{He} = 0$.

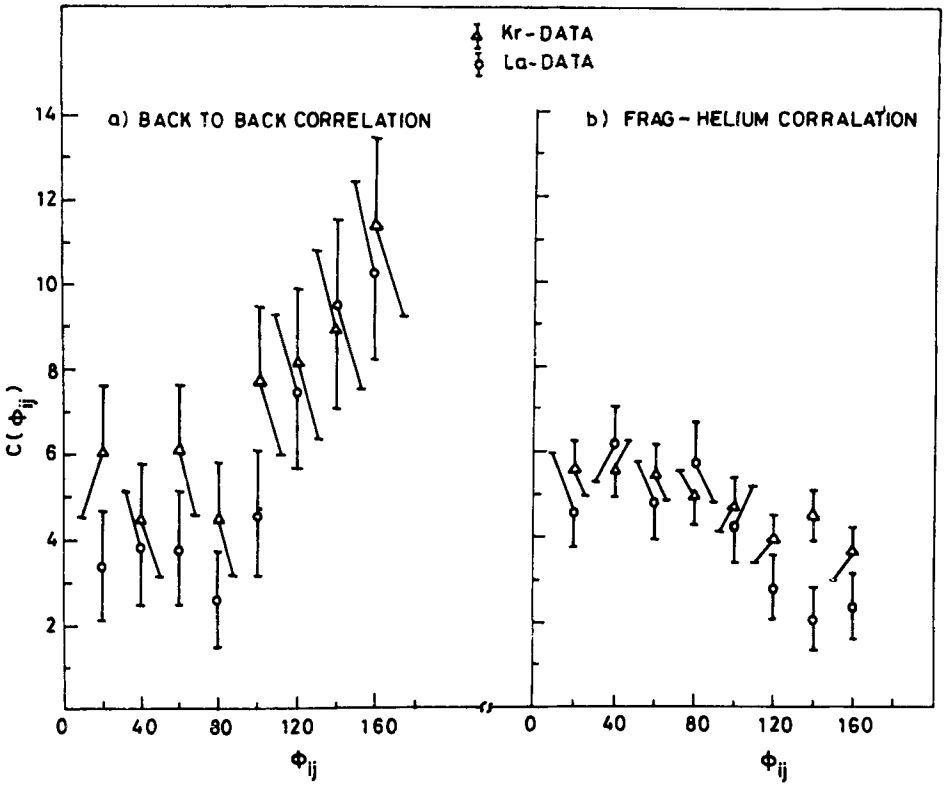

Figure 4. (a) Azimuthal angle correlation function $C(\Phi_{ij})$ plotted for bounce-off projectile and target nuclei using data of their principal vectors and (b) same two prong correlation function in between helium and heavier fragments ($Z \geqslant 3$) emitted from the bounce-off projectile.

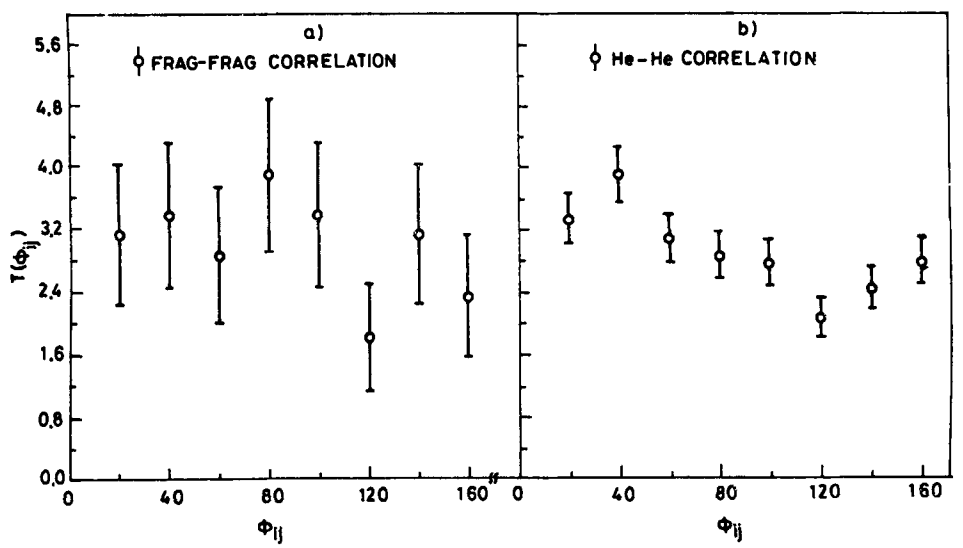

Figure 5. Azimuthal angle correlation function $T(\Phi_{ij})$ versus Φ_{ij} plot for (a) fragment–fragment and (b) helium-helium in the case of bounce-off events of La + Ag(Br) reaction.

was originally used for the study of proton-proton correlation. Before making its use for helium, heavier fragment correlation we have tested it for back-to-back correlation of La and Kr projectiles on Ag(Br) target. The results are given in figure 4a for both the reactions. The strong back-to-back correlation between projectile and target nuclei as seen earlier in figure 1 is evident from the correlation function $C(\Phi_{ij})$ also. Further, in figure 4b function $C(\Phi_{ij})$ has been plotted for fragment ($Z \geqslant 3$)—helium correlation for the two reactions. The data show a depression beyond $\Phi_{ij} > 80°$. It may be inferred that the heavier and helium fragments are correlated at small Φ_{ij} values. When both were emitted from one thermalised source then they were uncorrelated like the evaporated protons from a fire-ball.

In figures 5a and b, $T(\Phi_{ij})$ versus Φ_{ij} plots have been made for fragment-fragment and helium-helium pairs respectively. It may be seen from the figure that frag-frag correlation is almost absent except at $\Phi_{ij} \approx 90°$ and the source of fragments seems to behave like a fire ball. The abnormal peak at $\Phi_{ij} = 90°$ may be due to the squeeze out. There is a clear existence of helium-helium correlation at small Φ_{ij}.

4. Conclusions

(i) From the data of projected angle distribution given in table 2 for helium and heavier fragments ($Z \geqslant 3$) separately for the two reactions it is clear that there are significant differences in two categories of fragments. The difference is more in La + Ag(Br) than Kr + Ag(Br) reaction. Data corresponding to helium fragments are closer to the Gaussian distribution as compared to the data of heavier fragments. This result indicates that at some stage of fragmentation, statistically speaking, there might be two chunks of nucleus with different physical conditions. One gives rise predominantly to light fragments like helium and other to heavier fragments. From the study of fragment-fragment and helium-helium correlation function plotted in figures 5a and b respectively the difference becomes more clear. From the data of $\bar{N}_{He}$ given in table 3 and the momentum widths given in table 4, it can be pointed out that momentum width increases with decrease of helium multiplicity-an effect seen in case of 200 A GeV O^{16} + Em collision by Adamovich *et al* [20]. This may be because of the emission of helium fragments from a relatively more compressed part of nucleus on reduction of the impact parameter. Based on this we have been able to show that average density of the compressed part is $\approx 4{\cdot}7$ times that of the uncompressed nucleus.

(ii) From the result given in § 3·2, regarding the three categories of events it is noted that bounce-off effect is prevalent even at smaller impact parameter [category (i)] though with reduced intensity. The big participant nuclear chunk experiences compression and as a result of fast randomization of longitudinal energy the excitation energy and the temperature are increased. The momentum distribution is also highly modified compared to large impact parameter collision. The high value of $\bar{\theta}_{PF}$ in category (i) compared to categories (ii) and (iii) may be conjectured as due to the rescattering. According to Stocker *et al* [21] the heating effects may mask the collective motion and our data of $\overline{\Delta\Phi}$ also supports this e.g. events of category (i) correspond to high temperature $\tau \approx 31$ MeV [$\tau = (2/3) \times (E^*/A)$] and smaller values of $\overline{\Delta\Phi}$ and R compared to events of category (iii) with temperature $\tau \approx 17$ MeV and values of $\overline{\Delta\Phi}$ and R being higher.

Acknowledgements

The author (BS) is grateful to the UGC and another author (HSP) to CSIR (New Delhi) for research fellowships. Thanks are also due to TWAS (ICTP, Italy) research grants. Authors are thankful to Prof. I. Otterlund (Sweden) for the emulsion stack.

Appendix

Fermi momentum, P_F and nucleon density, ρ of normal nuclear matter are related as,

$$P_F = [(3/2) \times (\hbar^3 \pi^2 \rho)]^{1/3}$$

or

$$P_F \propto \rho^{1/3}. \tag{A1}$$

According to Feshbach and Huang [22] momentum square average to the first approximation can be written in terms of Fermi-momentum square,

$$\langle P^2 \rangle = \frac{3}{5} P_F^2 \tag{A2}$$

and for a fragment of given mass, square of the width of the momentum distribution, σ^2 is shown [22, 23] to be proportional to $\langle P^2 \rangle$ i.e.

$$\sigma^2 \propto \langle P^2 \rangle. \tag{A3}$$

In this way σ^2 can be shown to vary with the nuclear density as follows,

$$\sigma^2 \propto \rho^{2/3}$$

or

$$\sigma \propto \rho^{1/3} \tag{A4}$$

It is well-known from the shock wave model of nuclear collisions [17] that at projectile energies 1 to 2 GeV/nucleon resonances affect the density of nuclear matter by an amount which is much smaller than the order of magnitude. Considering that at these energies during the compression nuclear matter does not lose its identity one can therefore make use of the relation (8) for estimating the nuclear density in terms of the width, σ of the projected momentum distribution as explained in the § 3·2.

References

[1] H A Gustafsson, H H Gutbrod, B Kolb, H Lohner, B Ludewigt, A M Poskanzer, T Renner, H Riedesel, H G Ritter, A Warwick, F Weik and H Wieman, *Phys. Rev. Lett.* **52**, 1590 (1984)

[2] H G Ritter, K G R Doss, H A Gustafsson, H H Gutbrod, K H Kampert, B Kolb, H Lohner, B Ludewigt, A M Poskanzer, A Warwick and H Wieman, *Nucl. Phys.* **A447**, 3C (1985)

[3] D Beavis, S Y Chu, S Y Fung, W Gorn, A Huie, D Keane, J J Lu, R T Poe, B C Shen and G Vandalen, *Phys. Rev.* **C27**, 2443 (1983)

[4] R E Renfordt, D Schall, R Bock, R Brockmann, J W Harris, A Sandoval, R Stock, H Strobele, D Bangert, W Rauch, G Odyniec, H G Pugh and L S Schroeder, *Phys. Rev. Lett.* **53**, 763 (1984)

[5] A Sandoval, R Stock, H E Stelzer, R E Renfordt, J W Harris, J P Brannigan, J V Geaga, L J Rosenberg, L S Schroeder and K J Wolf, *Phys. Rev. Lett.* **45**, 874 (1980)

[6] H G Baumgardt, J U Schoot, Y Sakamoto, E Schopper, H Stocker, J Hofmann, W Scheid and W Greiner, *Z. Phys.* **A273**, 359 (1975)
[7] H H Heckmann, Y J Karant and E M Friedlander, *Phys. Rev.* **C34**, 1333 (1986)
[8] R Arora and V Kumar *et al Z. Phys.* **A333**, 373 (1989)
[9] W Scheid, H Muller, M Greiner, *Phys. Lett.* **32**, 741 (1974)
[10] A A Amsden, G F Bertsch, F H Harlow and J R Nix, *Phys. Rev. Lett.* **35**, 905 (1975)
[11] J Cugnon and D L'Hote, *Nucl. Phys.* **A447**, 27C (1985)
J Cugnon *et al Phys. Rev.* **C35**, 861 (1987)
E Braun and Z Fraenkel, *Phys. Rev.* **C34**, 120 (1986)
[12] J Gosset, H H Gutbrod, W G Meyer, A M Poskanzer, A Sandoval, R Stocker and G D Westfall, *Phys. Rev.* **C16**, 629 (1977)
[13] H Stocker, G Buchwald, G Graebner, P Subramanian, J A Maruhn, W Greiner, B V Jacak and G D Westfall, *Nucl. Phys.* **A400**, 63C (1983)
[14] H S Palsania, B Singh, A Gill, V Kumar, K B Bhalla and S Lokanathan, *Mod. Phys. Lett.* **A6**, 2757 (1991)
[15] H Kallies *et al*, Private communication, Marburg University, Oct. (1989)
[16] H Stocker, M Gyulassy and J Boguta, *Phys. Lett.* **B103**, 269 (1981)
[17] H Stocker, J Hofmann, J A Maruhn and W Greiner, *First Workshop on ultra-relativistic nuclear collisions*, **LBL-8957**, 355 (1979)
[18] S E Koonin, *Phys. Rev. Lett.* **39**, 680 (1977)
[19] B Jakobsson, *Phys. Scr.* **17**, 491 (1978)
[20] Adamovich *et al*, *Phys. Rev.* **C40**, 66 (1989)
[21] H Stocker, M Gyulassy and J Boguta, *Phys. Lett.* **B103** 269 (1981)
[22] H Feshbach and K Huang, *Phys. Lett.* **B47**, 300 (1973)
[23] A S Goldhaber, *Phys. Lett.* **B53**, 306 (1974)